# Structural Transformation and Melting in Gold Shock Compressed to 355 GPa

Surinder M. Sharma, Stefan J. Turneaure, J. M. Winey, Yuelin Li, Paulo Rigg, Adam Schuman, Nicholas Sinclair, Y. Toyoda, Xiaoming Wang, Nicholas Weir, Jun Zhang, and Y. M. Gupta

Phys. Rev. Lett. **123**, 045702 — Published 24 July 2019

DOI: 10.1103/PhysRevLett.123.045702

**Structural transformation and melting in gold shock-compressed to 355 GPa**

Surinder M. Sharma[1], Stefan J. Turneaure[1], J. M. Winey[1], Yuelin Li[2,3], Paulo Rigg[2], Adam Schuman[2], Nicholas Sinclair[2], Y. Toyoda[1], Xiaoming Wang[2], Nicholas Weir[2], Jun Zhang[2] and Y. M. Gupta[1,4]

[1]Institute for Shock Physics, Washington State University, Pullman, Washington 99164, USA
[2]Dynamic Compression Sector, Institute for Shock Physics, Washington State University, Argonne, Illinois 60439, USA
[3]Advanced Photon Source, Argonne National Laboratory, Argonne, IL 60439 USA
[4]Department of Physics and Astronomy, Washington State University, Pullman, Washington 99164, USA

**Abstract:**

Gold is believed to retain its ambient crystal structure to very high pressures under static and shock compression, enabling its wide use as a pressure marker. Our *in situ* x-ray diffraction measurements on shock-compressed gold show that it transforms to the body-centered-cubic (bcc) phase, with an onset pressure between 150-176 GPa. Liquid/bcc coexistence was observed between 220-302 GPa and complete melting occurs by 355 GPa. Our observation of the lower coordination bcc structure in shocked gold is in marked contrast with theoretical predictions and the reported observation of the hexagonal-close-packed structure under static compression.

It is commonly accepted that materials adopt unique equilibrium crystal structures for given thermodynamic conditions (pressure and temperature values). Unlike the nearly isotropic strains encountered under static high pressure compression, shock wave compression results in states of uniaxial strain. Nevertheless, the crystal structures attained under shock compression have an almost one to one correspondence with the static compression phases [1-5]. Because shock compression can generate pressure-temperature conditions not easily accessible under static compression, there is the potential to discover new structures not observable under static compression.

Gold, considered the noblest metal [6] and widely used for a variety of purposes over the centuries, is known to exist in the close packed face centered cubic (fcc) structure at ambient conditions. Because its ambient structure stays stable up to almost a terapascal [7] under static compression and because of its non-reactive properties, gold is a popular pressure marker in diamond anvil cell (DAC) based high pressure experiments [8-10]. Gold also retains its fcc structure up to its melting temperature, which is known to increase with pressure [11]. Under shock compression, Hugoniot measurements on Au have not identified any features that can be ascribed to phase transitions, including melting, up to 580 GPa in gas gun experiments [12] and up to 10 TPa in laser shock experiments [13].

Evaluation of the Au structural stability limits has been a topic of considerable theoretical interest. Based on first principles total energy calculations, the fcc phase was predicted to become unstable compared to the hexagonal close packed (hcp) phase beyond ~ 200-240 GPa [14, 15] or 350-410 GPa [16]; the exact value depends on the computational method used. Commenting on Ref. [14], Soderlind predicted transformation to hcp at ~151 GPa [17]. Later theoretical investigations suggest an evolving stacking order beyond the predicted stability field

of fcc (> 200 GPa), leading to a double hexagonal close packed structure before transforming to the hexagonal close packed structure [18,19]. These changes are predicted to take place over a stress range of 200-700 GPa (the predicted onset pressure for hcp phase is ~ 420-710 GPa [18] or ~448 GPa [19], depending on the computational method used). At higher temperatures (> 2000 K), an fcc-bcc phase transformation has also been predicted [15]. In contrast, under shock compression the fcc phase is predicted to undergo only one structural modification, namely melting. However, the pressures at which shock-induced melting is predicted to occur differ significantly for the different studies: 120 GPa [20], 210 GPa [15], or 280 GPa [21].

Experimental work has led to contradictory conclusions regarding the structural stability of gold under static high pressures. The fcc structure has been found to persist in gold to pressures reaching a terapascal [7]. However, an earlier study claimed observation of the hcp phase beyond 240 GPa over a limited range of pressures and temperatures [22] (between 230-275 GPa and 300-500 K). Compression of the fcc-hcp mixed phase at high temperatures (600-800 K) was reported to result in full reconversion to the fcc phase [22].

To determine if gold undergoes any structural phase transitions under shock compression, we have carried out *in situ* x-ray diffraction (XRD) measurements up to 355 GPa. Our experimental results have established unambiguously two structural phase transitions under shock compression: fcc to bcc transformation onset between 150-176 GPa, and the onset of melting of the bcc structure by 220 GPa.

The *in situ* XRD experiments were performed at the laser-shock experiment station [23] of the Dynamic Compression Sector (DCS), located at the Advanced Photon Source. The configuration of the experiments is shown schematically in Fig. 1. A 5 or 10 ns pulse duration 100 J laser was used to ablate an aluminized Kapton film, resulting in a shock wave in the

Kapton which propagated into a nominally 8 μm thick gold foil obtained from Goodfellow; the foil was fully dense ($\rho_0$ = 19.30 g/cc) and 99.9% pure. Different laser pulse shapes and energies were used to generate flat-top shocked states in the Au samples with nominal stresses near 150, 175, 220, 230, 270, 300 and 355 GPa. Velocity interferometry (VISAR) [24] was used to record the particle velocity histories at the gold/LiF window interfaces, at a location centered on the 500 μm laser-drive spot. More details about the laser-shock experimental capabilities at DCS can be seen in Ref. [23].

A typical gold/LiF particle velocity history under shock compression is shown in Figure 1b, which displays a constant particle velocity for a few nanoseconds behind the shock wave, corresponding to a constant stress state. Measured gold/LiF particle velocity histories for all 11 experiments performed are shown in Supplementary Materials (SM) Fig. S1 [25]. Shock stresses and other results for each experiment are listed in Supplementary Materials (SM) Table S1 [25].

Powder XRD patterns were recorded on an area detector, capturing the first five complete diffraction rings of ambient gold in the fcc structure [25]. The XRD measurements consist of a single snapshot obtained using a ~100 ps duration x-ray pulse with a bandwidth of a few percent and maximum x-ray flux at ~23.5 keV. During most of the experiments, the XRD pattern was recorded while the high-stress (150-355 GPa) shock wave was propagating through the Au sample, before the shock reflected from the LiF window. For these experiments, a small fraction of the ambient Au XRD pattern was superposed on the XRD pattern for shocked Au. Table S1 lists the fraction of unshocked material observed in each experiment [25]. XRD patterns were converted to one-dimensional line profiles by integrating around the rings. To obtain the XRD line profile arising from the shocked gold, the appropriate fraction of the ambient XRD line profile was subtracted [25].

Representative XRD line profiles for ambient gold and for gold shocked to five different peak stresses are shown in Fig. 2. Our results show that Au maintains the fcc structure under shock compression up to 149 GPa. However, beyond that stress, the nature of the diffraction pattern changes dramatically, giving rise to new peaks. The XRD profile at 176 GPa is not indexable to either the fcc structure or the hcp structure, which has been suggested as a high pressure structure based on theoretical predictions [14-19] and on diamond anvil cell experiments [22]. Instead, the measured diffraction pattern can be indexed to a mixture of fcc and bcc phases. For 220 GPa and higher pressures, the $(220)_{fcc}$ peak is not discernible, implying that Au is fully transformed to the bcc phase. At ~ 220 GPa, the dominant $(110)_{bcc}$ peak rides on top of a broad hump, suggesting the onset of melting. Around 300 GPa, the diffraction features of the molten phase are dominant and bcc peaks at higher angles become weak and significantly broadened. Persistence of the sharp $(110)_{bcc}$ peak implies coexistence of bcc and molten phase up to this stress. The diffraction pattern at 355 GPa (Figs. 1d and 2) represents the fully molten state.

Lattice parameters for the bcc and fcc structures were determined by comparing the measured XRD line profiles with simulated profiles. Simulated line profiles for shocked gold, shown as the red curves in Fig. 2, contain an fcc XRD simulation (149 GPa), a mixture of fcc and bcc XRD simulations (176 GPa) or a mixture of bcc XRD simulations and a liquid scattering line profile (220-302 GPa). We also note that the diffraction peaks for shocked Au are somewhat broader than the ambient peaks, suggesting possible smaller coherently diffracting domains in the shocked material and/or broadening due to deformation induced defects [31]. If broadening due to defects is ignored, then the simulated $(110)_{bcc}$ peak widths and the Scherrer equation [31] suggest a lower bound of ~6 nm for the bcc Au coherently diffracting domains. However, there

is additional hkl-dependent broadening of other peaks which cannot be explained by size broadening alone. In particular, the measured $(211)_{bcc}$ peaks are significantly broader than the simulated $(211)_{bcc}$ peaks suggesting that defects in the bcc structure are responsible for a portion of the line broadening. Figure 2 shows the simulations that provide the best match to the measured line profiles. The simulations are discussed in more detail in SM [25].

The volume compressions ($V/V_0$) for shocked gold, determined from the present XRD experiments, are shown in Fig. 3. The measured values agree well with the Hugoniot curve obtained from continuum studies [12,26,27]. Our observations imply an extremely small volume change across the fcc-bcc phase transformation. This is consistent with the absence of any significant observable discontinuity in the Hugoniot data [12,26,27]. In addition, the co-existence of the bcc phase and the molten phase between 220-300 GPa – over almost 80 GPa – is consistent with the previous report [12] of a smooth Hugoniot curve across the melting transformation.

Our observation of the bcc phase in Au shock-compressed to 176 – 302 GPa differs qualitatively from expectations based on previous experimental [7,22] and theoretical [14,16-21] work. Although recent theoretical calculations [15] predict an fcc-bcc phase boundary at high pressure–high temperature conditions – that have not yet been explored experimentally – these same calculations predict that the fcc phase is the only stable solid phase in the regions of phase space accessible by shock wave compression (i.e. along the Hugoniot curve), with melting predicted at higher shock pressures. Therefore, the results presented here show that theoretical predictions for the phase diagram of gold at high pressures and high temperatures need to be revisited.

For pressure-induced phase transformations, the initial structures are typically expected to transform to structures having either comparable or higher coordination number, because the high pressure phase must be denser than the low pressure phase. In that sense, the previous theoretical calculations that predict an fcc-hcp transformation at high pressures are reasonable because the fcc and hcp structures both possess 12-fold coordination. In contrast, our experimental observation of an fcc-bcc transformation under compression is counter-intuitive, as the bcc structure has a lower coordination number (8) than the initial fcc structure. Structural changes to lower coordination under compression are known to occur due to underlying severe changes in the electronic states [32,33]. In such cases, the lower coordination structures are also expected to be observed under static pressures, as has been observed in Mg [34] and Ca [35]. Calculations on Au, similar to [32, 33], suggest the possibility of the bcc phase at pressures greater than 400 GPa [17] or 1360 GPa [18] (Note that Ref. [17] might provide a severe underestimate as it predicted an fcc-hcp phase change at 151 GPa). However, the observed stability of the fcc structure under static pressure up to 1 TPa [7] suggests that other factors may play a crucial role. Two possible factors, both inherent to shock wave compression, are large temperature increases and generation of lattice defects. If the bcc phase is entropy-stabilized [15], then the fcc-bcc transformation should, in principle, be observable in static high pressure – high temperature experiments. However, our results, together with previous EOS calculations [15, 21], suggest that the bcc phase appears in shocked Au at temperatures greater than 4000 K; such conditions are challenging to achieve under static compression [36,37]. Alternatively, because the uniaxial strain condition inherent to shock compression typically results in copious lattice defects in fcc metals [38], it is possible that the fcc-to-bcc phase transformation presented

here is strongly facilitated by these defects [39]. In such a case, the fcc-to-bcc transformation might be observable only under shock wave loading conditions and not under static compression.

Although the fcc-bcc structural phase transition is counter intuitive, the melting transition observed at higher stresses – due to the concomitant temperature increase under shock compression – is consistent with previous similar observations of melting in shocked Si and Ge using *in situ* XRD [5,40,41]. Observed co-existence of the bcc phase and the molten state implies that the onset of melting in shocked Au is ~ 220 GPa. This onset stress is closer to the prediction of Smirnov (210 GPa) [15] than that of Greef and Graf (280 GPa) [21], and differs substantially from the earlier estimate of Godwal, et al. (~120 GPa) [20]. However, the experimental results presented here are fundamentally different from the theoretical calculations in that the experimental observations represent melting from the bcc structure, while the theoretical results address melting from the fcc phase.

Studies of the fcc-bcc phase transformation in steels, where the transformation arises due to changes in temperature, suggest that this phase change can occur through a displacive mechanism, such as the Bain [42], Kurdjumov–Sachs [43], or Nishiyama–Wasserman [44] path. The operative transformation mechanism in gold can, in principle, be identified through *in situ* measurements of the orientation relations.

**Acknowledgements**

This publication is based upon work supported by the U.S. Department of Energy (DOE), National Nuclear Security Administration (NNSA) under Award Number DE-NA0002007. This publication is also based upon work performed at the Dynamic Compression Sector, which is

operated by Washington State University under DOE/NNSA Award Number DE-NA0002442. This research used resources of the Advanced Photon Source, a DOE Office of Science User Facility operated for the DOE Office of Science by Argonne National Laboratory under Contract No. DE-AC02-06CH11357.

**References:**


[1] G. E. Duvall and R. A. Graham, Rev. Mod. Phys. **49**, 523 (1977).

[2] D. H. Kalantar, *et al.*, Phys. Rev. Lett. **95**, 075502 (2005).

[3] S. J. Turneaure, N. Sinclair, and Y. M. Gupta, Phys. Rev. Lett. **117**, 045502 (2016).

[4] P. Kalita, P. Specht, S. Root, N. Sinclair, A. Schuman, M. White, A. L. Cornelius, J. Smith, and S. Sinogeikin, Phys. Rev. Lett. **119**, 255701 (2017).

[5] E. E. McBride, *et al.*, Nat. Phys. **15**, 89 (2019).

[6] B. Hammer and J. K. Norskov, Nature **376**, 238 (1995).

[7] N. Dubrovinskaia, *et al.*, Sci. Adv. **2**, e1600341 (2016).

[8] D. L Heinz and R. Jeanloz, J. Appl. Phys. **55**, 885 (1984).

[9] A. Dewaele, P. Loubeyre, and M. Mezouar, Phys. Rev. B **70**, 094112 (2004).

[10] K. Takemura and A. Dewaele, Phys. Rev. B **78**, 104119 (2008).

[11] L. H. Cohen, W. Klement, Jr., and G. C Kennedy, Phys. Rev. **145**, 519 (1966).

[12] M. Yokoo, N. Kawai, K. G. Nakamura, and K. Kondo, Appl. Phys. Lett. **92**, 051901 (2008).

[13] D. Batani, A. Balducci, D. Beretta, A. Bernardinello, T. Lower, M. Koenig, A. Benuzzi, B. Faral, and T. Hall, Phys. Rev. B **61**, 9287 (2000).

[14] R. Ahuja, S. Rekhi, and B. Johansson, Phys. Rev. B **63**, 212101 (2001).

[15] N. A. Smirnov, J. Phys.: Condens. Matter **29,** 105402 (2017).

[16] J. C. Boettger, Phys. Rev. B **67**, 174107 (2003).

[17] P. Soderlind, Phys. Rev. B **66**, 176201 (2002).

[18] T. Ishikawa, K. Kato, M. Nomura, N. Suzuki, H. Nagara and K. Shimizu, Phys. Rev. B **88**, 214110 (2013).

[19] Z. L. Liu, Y. P. Tao, X. L. Zhang and L. C. Cai, Comp. Mater. Sci. **114**, 72 (2016).

[20] B. K. Godwal, L. Ng and L. Dasilva, Phys. Lett. A **144**, 26 (1990).

[21] C. W. Greeff and M. J. Graf, Phys. Rev. B **69**, 054107 (2004).

[22] L. Dubrovinsky, N. Dubrovinskaia, W. A. Crichton, A. S. Mikhaylushkin, S. I. Simak, I. A. Abrikosov, J. S. de Almeida, R. Ahuja, W. Luo, and B. Johansson, Phys. Rev. Lett. **98,** 045503 (2007).

[23] X. Wang, *et al.*, Rev. Sci. Instrum. **90**, 053901 (2019).

[24] L. M. Barker and R. E. Hollenbach, J. Appl. Phys. **43**, 4669 (1972).

[25] See Supplemental Material at […] for a table of experimental results, additional velocity interferometry results, and a description of the XRD analysis methods. Supplemental Material includes Refs. [26-30].

[26] *LASL Shock Hugoniot Data*, edited by S. P. Marsh (University of California Press, Los Angeles, 1980), p. 81.

[27] L. V. Altshuler, A. A. Bakanova, I. P. Dudoladov, E. A. Dynin, R. F. Trunin and B. S. Chekin, J. Appl. Mech. Tech. Phys. **22,** 145 (1981).

[28] P. A. Rigg, M. D. Knudson, R. J. Scharff and R. S. Hixson, J. Appl. Phys. **116**, 033515 (2014).

[29] A. P. Hammersley, S. O. Svensson, M. Hanfland, A. N. Fitch and D. Hausermann, High Pressure Res. **14**, 235 (1996).

[30] A. P. Hammersley, *FIT2D: An introduction and overview*. ESRF Internal Report No. ESRF97HA02T (1997).

[31] B. E. Warren, X-ray Diffraction (Addison-Wesley, Reading, 1969).

[32] John A. Moriarty and A. K. McMahan, Phys. Rev. Lett. **48**, 809 (1982).

[33] R. Ahuja, O. Eriksson, J. M. Wills and B. Johansson, Phys. Rev. Lett. **75**, 3473 (1995).

[34] G. W. Stinton, S. G. MacLeod, H. Cynn, D. Errandonea, W. J. Evans, J. E. Proctor, Y. Meng and M. I. McMahon, Phys. Rev. B **90**, 134105 (2014).

[35] H. Olijnyk and W. B. Holzapfel, Phys. Lett. A **100**, 191 (1984).

[36] S. Petitgirard, A. Salamat, P. Beck, G. Weck and P. Bouvier, J. Synchrotron Rad. **21**, 89 (2014).

[37] R. Giampaoli,I. Kantor, M. Mezouar, S. Boccato, A. D. Rosa, R. Torchio, G. Garbarino, O. Mathon and S. Pascarelli, High Press. Res. **38**, 250 (2018).

[38] B. L. Holian and P. S. Lomdahl, Science **280**, 2085 (1998).

[39] Y. Gao and Y. Wang, Phys. Rev. Materials **2**, 093611 (2018).

[40] S. J. Turneaure, S. M. Sharma and Y. M. Gupta, Phys. Rev. Lett. **121**, 135701 (2018).

[41] P. Renganathan, S. J. Turneaure, S. M. Sharma and Y. M. Gupta, Phys. Rev. B **99**, 134101 (2019).

[42] E. Bain, Trans. Am. Inst. Min. Metal. Pet. Eng. **70**, 25 (1924).

[43] G. V. Kurdjumov and G. Sachs, Z. Phys. **64**, 325 (1930).

[44] Z. Nishiyama, Sci. Rep. Tohoku Imp. Univ. **23**, 637 (1934).

Figure Captions

1. (Color online) Experimental configuration and representative results. (a) Schematic of the configuration for *in situ* continuum and x-ray diffraction measurements in laser shocked Au. (b) Representative measured Au/LiF window interface velocity history showing a flat-top shocked state. (c) Representative XRD pattern measured for Au shock-compressed to 220 GPa. Diffraction rings corresponding to the bcc structure are dominant. However, ambient fcc diffraction rings remain visible since ~15% of the material was still unshocked at the time of the x-ray diffraction measurement. (d) X-ray diffraction pattern showing a liquid scattering ring for Au fully shocked to 355 GPa.

2. (Color online) Representative measured and simulated XRD line profiles for ambient and laser-shocked gold samples. The thick black lines are measured line profiles with background subtracted. For shocked state line profiles, the contribution from unshocked Au was also subtracted. The thin red lines are simulated line profiles using fcc and/or bcc lattice parameters that give the best match between simulated and measured profiles. Simulated line profiles for shock stresses 220 GPa or higher included a contribution from liquid scattering [25]. No simulation is shown for the 355 GPa experiment since crystalline peaks were not observed. Peaks corresponding to the fcc (bcc) structure are listed with pink (green) indices and features due to liquid scattering are identified by blue arrows.

3. (Color online) Stress vs. volume for shock-compressed gold. The pink diamond shows the volume for fcc Au at 149 GPa. The green circles show the volumes for bcc Au. The volumes were determined from the measured XRD data; the stresses were determined from the measured velocity profiles at the Au/LiF interface [25]. The gray band is the Hugoniot curve based on continuum measurements from Refs. [12,26,27]; the uncertainty in the curve is indicated by the width of the band.

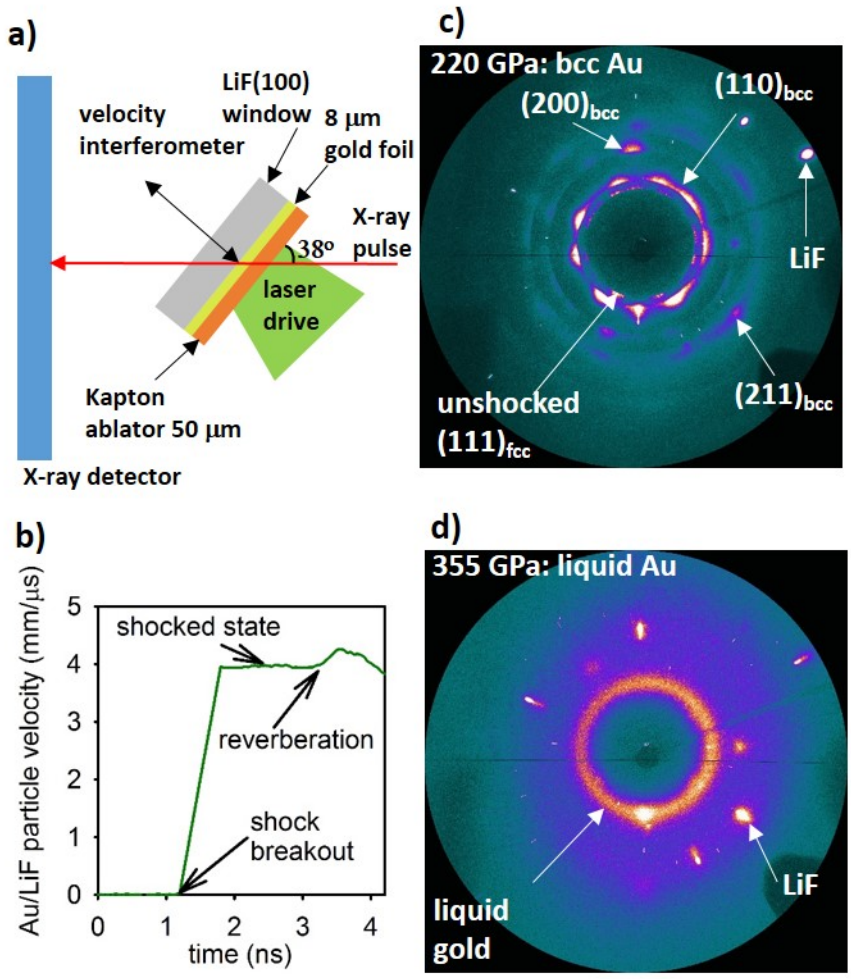
a)
LiF(100)
window
velocity
interferometer
8 μm
gold foil
X-ray
pulse
38°
laser
drive
Kapton
ablator 50 μm
X-ray detector
b)
Au/LiF particle velocity (mm/μs)
shocked state
reverberation
shock
breakout
time (ns)
c)
220 GPa: bcc Au
(200)bcc
(110)bcc
LiF
unshocked
(111)fcc
(211)bcc
d)
355 GPa: liquid Au
LiF
liquid
gold

**Figure 1**

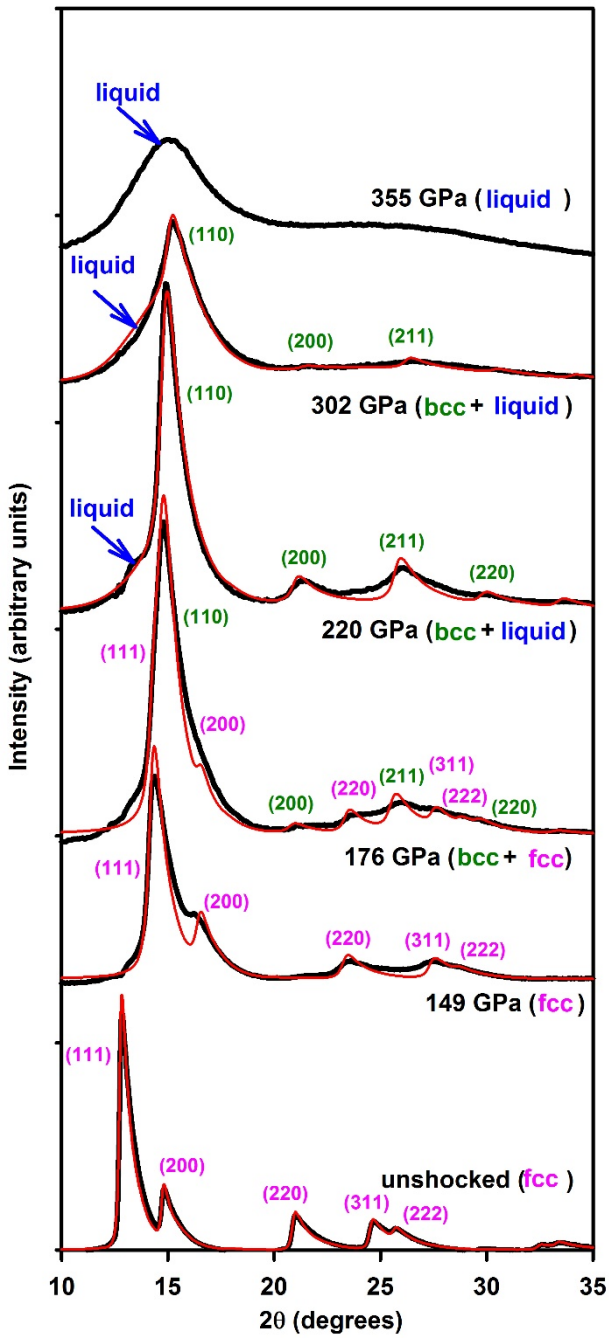
liquid
355 GPa ( liquid )
(110)
liquid
(200)
(211)
302 GPa (bcc + liquid )
(110)
liquid
(200)
(211)
(220)
220 GPa (bcc + liquid)
(111)
(110)
(200)
(200)
(220)
(211)
(311)
(222)
(220)
176 GPa (bcc + fcc)
(111)
(200)
(220)
(311)
(222)
149 GPa (fcc )
(111)
(200)
(220)
(311)
(222)
unshocked (fcc )
Intensity (arbitrary units)
10
15
20
25
30
35
2θ (degrees)

**Figure 2**

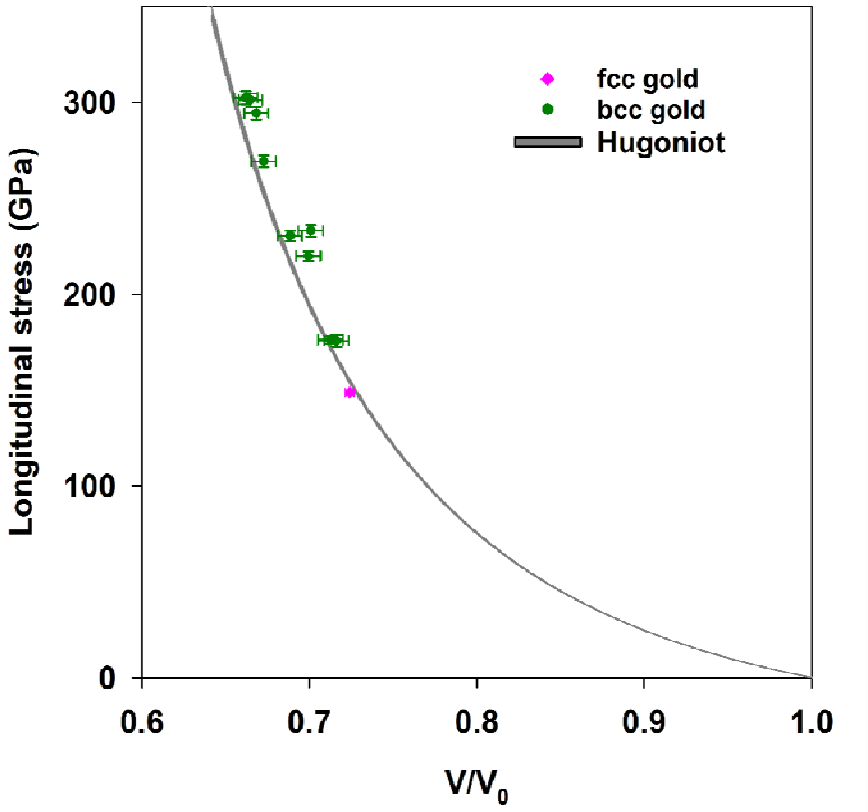
fcc gold
bcc gold
Hugoniot
Longitudinal stress (GPa)
300
200
100
0
0.6
0.7
0.8
0.9
1.0
V/V0

**Figure 3**